The Extension of Analytic Hypersonic Force Coefficients for Conceptual Design Using the Divergence Theorem

Michael J. Grant[*] and Robert D. Braun[†]

Georgia Institute of Technology, Atlanta, GA, 30332

This study investigates the type and performance of analytic Newtonian aerodynamic solutions made possible using the Divergence Theorem. A reformulation of the Newtonian surface pressure calculation enables a mathematically equivalent divergence calculation to be performed as a substitute. This manipulation enables analytic force coefficients to be derived for shapes of increasing complexity while also reducing computational cost when compared to existing analytic solutions. The divergence solutions are obtained by converting the physical flow field into a mathematical flow field that is constant in direction but with magnitude that is equivalent to the Newtonian pressure coefficient. This unique property allows various mathematical techniques that are not available with the traditional Newtonian calculation to be performed that further reduce computational cost. The results of this investigation enable the construction of analytic relations for new hypersonic configurations of interest, and this approach serves as the foundation to construct efficient hybrid exact-approximate solutions for more complex configurations. Comparisons of the current analytic database to a state-of-the-art hypersonic design tool illustrate the computational advantages of the analytic relations to support hypersonic conceptual design.

Nomenclature

APAS	Aerodynamic Preliminary Analysis System
CBAERO	Configuration Based Aerodynamics
CFD	Computational Fluid Dynamics
HABP	Hypersonic Arbitrary Body Program

A	panel area, m^2		$\mathbf{df}$	differential force, N
A_{ref}	reference area, m^2		$\mathbf{F}$	vector field
C_A	axial force coefficient		$\mathbf{\hat{n}}$	unit normal, m
C_N	normal force coefficient		$\mathbf{r}$	surface position vector, m
C_S	side force coefficient			
C_p	pressure coefficient		α	angle of attack, rad
D	volume domain		δ_c	cone angle, rad
p	pressure on surface of body, Pa		θ	relative angle between body and flow, rad
p_∞	freestream pressure, Pa		ρ	potential radius, m
r_n	nose radius, m		ρ_∞	freestream density, kg/m^3
S	surface domain		ϕ	potential function
V_∞	freestream velocity, m/s		ω	revolution angle, rad

---

[*]Graduate Research Assistant, Guggenheim School of Aerospace Engineering, AIAA Student Member.
[†]David and Andrew Lewis Associate Professor of Space Technology, Guggenheim School of Aerospace Engineering, AIAA Fellow.

I. Introduction

Traditionally, the hypersonic aerodynamics of vehicles are modeled during conceptual design using Newtonian flow theory.[1,2] This theory assumes that when a particle (traveling in rectilinear motion) strikes the surface of a body, all of the momentum normal to the surface would be lost and all momentum tangential to the surface would be conserved as shown in Figure 1. Consequently, the pressure exerted by the fluid on the surface of a body is assumed to be solely originating from this loss of momentum normal to the surface. Under these assumptions, the nondimensional pressure coefficient, C_p, at any point on the surface of a body can be obtained from the Newtonian sine-squared relation shown in Eq. (1). Furthermore, the pressure exerted by the fluid on any portion of the surface not directly exposed to the flow, denoted as the shadowed region of the body, is assumed to be equivalent to the freestream pressure in which the motion of the fluid does not influence the pressure in this region. Consequently, $C_p = 0$ throughout the shadowed region as shown in Figure 2.

$$C_p = \frac{p - p_\infty}{\frac{1}{2}\rho_\infty V_\infty^2} = 2\sin^2\theta \tag{1}$$
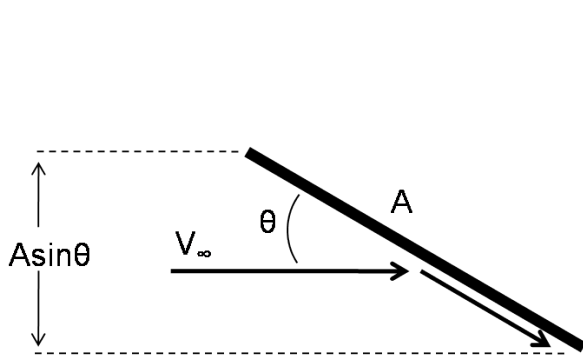

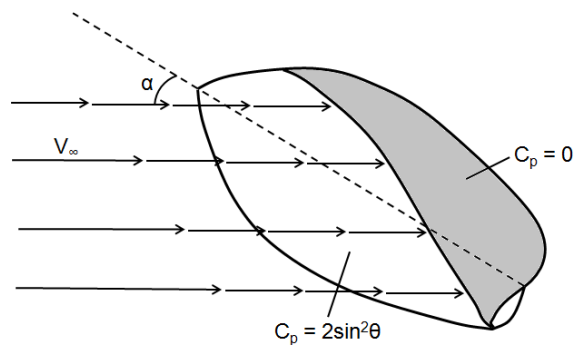Figure 1. Momentum transfer of particle on inclined surface.[2]

Figure 2. Example of shadowed body.[2]

The pressure that results from this momentum transfer is integrated over the unshadowed surface of the vehicle to calculate the hypersonic force coefficients as shown in Eq. (2), where $\hat{\mathbf{n}}$ is the unit normal and $\mathbf{df}$ is calculated from Eq. (3). In traditional conceptual design, this surface integration is approximated numerically in the form of panel methods such as those included within the Configuration Based Aerodynamics (CBAERO) tool[3] and the Aerodynamic Preliminary Analysis System (APAS).[4,5,6] Additionally, the aerodynamics of bodies of revolution have been calculated using ring approximation methods.[7,8,9] Although these conceptual numerical methods allow rapid aerodynamic calculations compared to computational fluid dynamics (CFD), this process must be repeated for any change in shape of the vehicle. Additionally, the resolution of the mesh must be addressed when using numerical methods. For example, the number of required panels to achieve a desired accuracy is generally unknown in the beginning of the meshing process. Consequently, multiple meshes of various resolutions must be evaluated until the convergence of aerodynamic coefficients is observed. The construction of a mesh for complicated shapes would also likely require modeling in a computer-aided design package. While certain tools such as CBAERO provide built-in routines to mesh bodies of revolution, other vehicle shapes must be meshed using external tools such as the GNU Triangulated Surface Library (GTS).[10] These time-consuming issues associated with panel methods limit the number of vehicle shapes analyzed during conceptual design.

$$\begin{bmatrix} -C_A \\ C_S \\ -C_N \end{bmatrix} = \frac{1}{A_{ref}} \iint_S \begin{bmatrix} \mathbf{df}^T\hat{\mathbf{x}} \\ \mathbf{df}^T\hat{\mathbf{y}} \\ \mathbf{df}^T\hat{\mathbf{z}} \end{bmatrix} = \frac{1}{A_{ref}} \iint_S C_p \begin{bmatrix} \hat{\mathbf{n_{in}}}^T\hat{\mathbf{x}} \\ \hat{\mathbf{n_{in}}}^T\hat{\mathbf{y}} \\ \hat{\mathbf{n_{in}}}^T\hat{\mathbf{z}} \end{bmatrix} dA \tag{2}$$

$$\mathbf{df} = C_p\,\hat{\mathbf{n}}\,dA \tag{3}$$

American Institute of Aeronautics and Astronautics

I.A.   Motivation for Analytic Hypersonic Aerodynamics

While panel methods would likely be required for the conceptual design of complicated geometries such as the Space Shuttle Orbiter, X-38, and HL-20, many hypersonic vehicle designs used in previous and current mission studies are not complex. For example, all previous and currently planned Mars missions have used blunt sphere-cones. Various human Mars mission studies have used blunt sphere-cones and blunted biconics.[11,12,13] The Stardust and Genesis Earth entries also used blunt sphere-cones.[14,15] The Apollo and Orion command modules both utilized a spherical forebody segment. Many high performance military hypersonic vehicles are slender sphere-cones and slender biconics with minor nose blunting to account for extreme heating environments. Some high performance entry vehicles include blended wedge designs, such as the SHARP L1, that consist of flat plates, conical frustums, and nose blunting through a cylindrical segment.[16] These examples represent a subset of missions that implement relatively simple vehicle geometries, and Figure 3 illustrates the wide range of applications for these geometries.
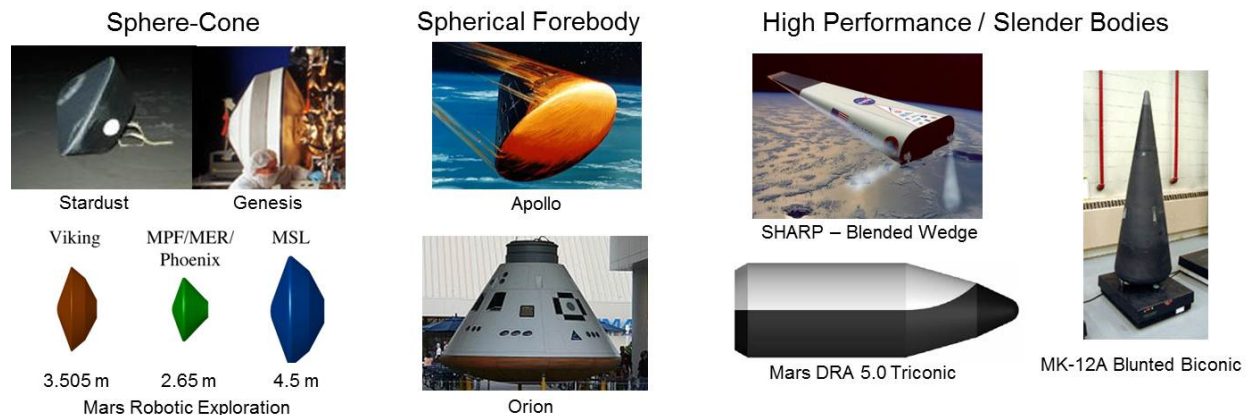

Figure 3. Example vehicles with analytic geometries.

The surface geometry of these basic shapes, along with additional complex shapes, can be expressed analytically. Consequently, the Newtonian surface integration that is traditionally performed numerically using panel methods can also be performed analytically. Many of the resulting analytic relations provide exact Newtonian aerodynamic coefficients currently approximated by panel methods. Additionally, the evaluation of most of the analytic relations is nearly instantaneous. As such, these relations could substitute panel methods widely used in traditional, segregated conceptual design environments to improve the computational performance of Newtonian aerodynamics calculations. More importantly, however, these relations eliminate the large aerodynamic tables that fundamentally segregate aerodynamics from other analyses during conceptual design and enable the construction of a unified, mathematical framework to perform rapid, simultaneous hypersonic aerodynamic and trajectory optimization.[17,18]

I.B.   Absence of Analytic Aerodynamics in Present-Day Analyses

The limited analytic relations developed in the 1950s and 1960s have largely been forgotten by the aerospace community in the recent decades. The manual development of analytic relations is time-intensive and requires complex integrations to be performed. As a result, the integration process is largely dependent on integral tables and appropriate substitutions, requiring substantial trial-and-error effort that is prohibitive during conceptual design. Rather, the advent of the digital computer resulted in the widespread adoption of panel and CFD methods over historical relations.[7,8,9,19,20,21,22,23] This can be observed by the many recent shape design studies that employ panel methods.[24,25]

Recent advances in symbolic manipulations tools, such as Mathematica[26] and Maple,[27] enable the modern construction of analytic relations for various shapes. These symbolic tools are capable of querying large databases of integral tables and substitution techniques, addressing some of the limitations that have historically prevented the adoption of analytic methods. Recent research has illustrated that the traditional Newtonian calculation can be performed analytically for a wide range of basic shapes, including conical frustums, spherical segments, cylindrical segments, and flat plates, and this research complements the historical analytic relations.[28] Many common hypersonic vehicles of interest, including those shown in Figure 3, can

American Institute of Aeronautics and Astronautics

be constructed through the superposition of these basic shapes. As such, the corresponding aerodynamics of each basic shape can also be combined to form analytic relations for vehicles of interest. This analytic aerodynamic database, that includes the analytic relations derived in this investigation, can be downloaded from the following file when viewed in Adobe Acrobat (aerodynamicsDatabase.zipREMOVEME)[a]. The enclosed Matlab routines should be referenced for the contents of the analytic expressions. When developing analytic relations, each vehicle is parametrized such that the resulting solutions must only be developed once and are valid across all configurations. This is a major advantage over panel methods that must be executed each time the shape of the vehicle changes. However, as the complexity of the shape of the vehicle increases, the analytic solutions also increase in complexity. For certain complex shapes, no analytic solution has currently been found and is a consequence of the fundamental challenges that exist within the traditional Newtonian calculation.

II.   Fundamental Challenges of Analytic Newtonian Aerodynamics

The most apparent challenge during the integration process is that many simple functions cannot be analytically integrated. For example, the function $\sin(x)/x$ has no known analytic integral. As vehicles of greater complexity are considered, no guarantee can be made regarding the existence of a closed form, analytic solution. In the most recent analytic work,[28] simple bodies of revolution are analyzed as an attempt to expand the database to include more complex shapes. The surface of these bodies is naturally parametrized using trigonometric functions of the revolution angle. For an example spherical segment that could serve as the nose of a sphere-cone vehicle with cone angle δ_c and nose radius r_n, the revolution angle, ω, shown in Figure 4 corresponds to the natural

Figure 4.   Side and front view of spherical segment parametrization.

surface parametrization as described by Eq. (4). As a result, the corresponding shadow boundaries that determine the limits of the analytic integration are functions of inverse trigonometric functions. These functions, when combined with other polynomial expressions that appear during the integration process, generally result in expressions that cannot be analytically integrated. For certain combinations that are analytically integrable, the solutions obtained by symbolic manipulation tools such as Mathematica generally result in very lengthy expressions that reduce computational performance.
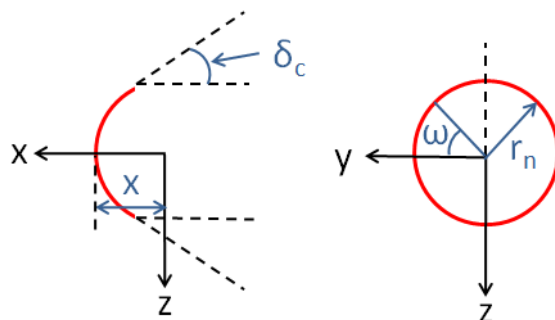
$$\mathbf{r} = [x \quad \sqrt{r_n^2 - x^2}\cos(\omega) \quad -\sqrt{r_n^2 - x^2}\sin(\omega)]^T \tag{4}$$

To avoid the complexity of inverse trigonometric functions, bodies of revolution could be parametrized using Cartesian coordinates. While this parametrization eliminates the inverse trigonometric functions that appear in the shadow boundary, alternate inverse trigonometric functions appear from the mapping of Cartesian distances (used to provide integration limits that the describe the surface of the shape) to inverse trigonometric functions during integration. An example of a simple distance calculation that results in an inverse trigonometric function is shown in Eq. (5). A similar phenomenon also exists due to the normal vector normalizations required to calculate the pressure coefficient and direction of force as shown in Eq. (3). As a similar example, the normalization term that appears in Eq. (6) also leads to an inverse trigonometric expression after integration. In fact, many vehicle configurations suffer from this inverse trigonometric complexity due to both of these complications.

$$\int \sqrt{1 - x^2}\,\mathrm{d}x = \frac{1}{2}(x\sqrt{1 - x^2} + \arcsin x) \tag{5}$$

$$\int \frac{1}{\sqrt{1 - x^2}}\,\mathrm{d}x = \arcsin x \tag{6}$$

---

[a]Prior to unzipping the file, the 'REMOVEME' portion of the file extension must be removed.

It is important to note that the spherical segment does not suffer from the complexity that results from vector normalizations since the magnitude of the normal vector is constant over the entire surface. Instead, this shape only suffers from the inverse trigonometric complexity that arises from the integration limits. If the terms that appear during the analytic integration process can be appropriately modified, then it is possible to avoid this complexity entirely for spherical segments. While solutions to spherical segments were obtained in prior work,[28] this new approach enables compact aerodynamic expressions to be constructed that reduce computational cost. Furthermore, this new approach enables the construction of analytic relations for more complex shapes and serves as a means to expand the analytic aerodynamic database. The necessary modification to the integration process can be achieved by departing from the traditional surface integration model of Newtonian flow theory to a volume integration using the Divergence Theorem.

III. Calculation of Newtonian Aerodynamics Using the Divergence Theorem

In traditional Newtonian flow theory, the aerodynamic coefficients are calculated by integrating the pressure coefficient over the unshadowed surface of the vehicle. In this model, the pressure coefficient is derived from the momentum transfer of fluid particles as they are deflected by the surface of the vehicle as shown in Figure 1. While this model is representative of the physics of the flow, it is mathematically equivalent to a flux that penetrates the surface of the vehicle with an assumed permeable outer mold line. As an example, the calculation of the normal force coefficient can be converted in this manner as shown in Eq. (7), where the flux does not originate from the physical fluid flow. Rather, a mathematical flow field is constructed, and the flux is calculated from this mathematical vector field. For the normal force coefficient calculation, the mathematical vector field is $\mathbf{F} = C_p\, \hat{\mathbf{z}}$ as shown in Eq. (7). Note that this mathematical vector field acts along $\hat{\mathbf{z}}$ only and is independent of the direction of the freestream flow as shown in Figure 5.
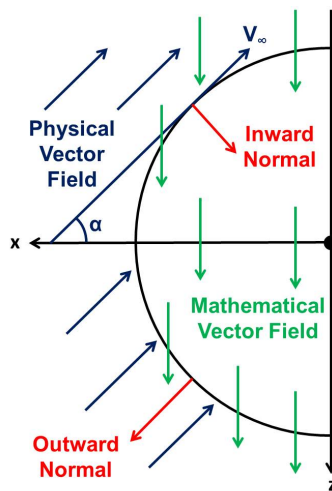

Figure 5. Comparison between physical and mathematical vector fields.

However, the magnitude of this mathematical vector field is equivalent to the pressure coefficient and, consequently, is a function of both vehicle shape and the relative orientation of the vehicle to the freestream flow. Although this calculation has never been previously performed for Newtonian flow, the mapping between interior and boundary calculations provided by the Divergence Theorem is similar to other aerodynamic applications that can be expressed using potential flow theory.[29]

$$
\begin{aligned}
C_N &= \frac{1}{A_{ref}} \iint_S C_p\, \hat{\mathbf{n}}_{\mathbf{in}}^T (-\hat{\mathbf{z}})\, \mathrm{d}A \\
&= \frac{1}{A_{ref}} \iint_S (C_p\, (-\hat{\mathbf{z}}))^T \hat{\mathbf{n}}_{\mathbf{in}}\, \mathrm{d}A \\
&= \frac{1}{A_{ref}} \iint_S (C_p\, \hat{\mathbf{z}})^T \hat{\mathbf{n}}_{\mathbf{out}}\, \mathrm{d}A
\end{aligned}
\tag{7}
$$

While this mathematical conversion does not change any calculations that would be made on the surface of the vehicle, it enables an alternate calculation to be performed using the Divergence Theorem. The Divergence Theorem is used to map the flux of a vector field, $\mathbf{F} = M\mathbf{i} + N\mathbf{j} + P\mathbf{k}$, across a closed oriented surface S in the direction of the surface's outward unit
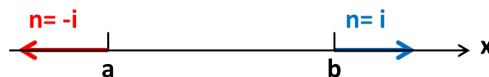

Figure 6. Outward unit normals at the boundary of $[a, b]$ in one-dimensional space.[30]

American Institute of Aeronautics and Astronautics

normal field, $\hat{\mathbf{n}}_{\mathbf{out}}$, to the divergence of the vector field $\mathbf{F}$ over the region D enclosed by the surface as shown in Eq. (8). Note that while the divergence form requires an additional integration to be performed, this is offset to a degree by the extra derivative of the integrand. The divergence form also eliminates the unit normal that generally increases the complexity of the integration process as described in Section II. As an example, the Fundamental Theorem of Calculus shown in Eq. (9) is a one-dimensional implementation of the Divergence Theorem. If $\mathbf{F} = f(x)\mathbf{i}$, then $\frac{\mathrm{d}f}{\mathrm{d}x} = \nabla^T \mathbf{F}$. By defining the outward unit normal to be $\mathbf{i}$ at b and $-\mathbf{i}$ at a as shown in Figure 6, then the total outward flux of $\mathbf{F}$ across the boundary of $[a, b]$ is equivalent to $f(b) - f(a)$ as shown in Eq. (10).[30] To compute the analytic force coefficients of various vehicles using the Divergence Theorem, this one-dimensional example is extended to three dimensions.

$$\iint\limits_{S} \mathbf{F}^T \mathbf{n}\,\mathrm{d}\sigma = \iiint\limits_{D} \nabla^T \mathbf{F}\,\mathrm{d}V \tag{8}$$

$$f(b) - f(a) = \int\limits_{a}^{b} \frac{\mathrm{d}f}{\mathrm{d}x} \tag{9}$$

$$\begin{aligned} f(b) - f(a) &= f(b)\mathbf{i}^T\mathbf{i} + f(a)\mathbf{i}^T(-\mathbf{i}) \\ &= \mathbf{F}(b)^T\mathbf{n} + \mathbf{F}(a)^T\mathbf{n} \end{aligned} \tag{10}$$

The transformation provided by the Divergence Theorem is of little use when numerically approximating the hypersonic force coefficients since the addition of a third integral would likely increase the computational requirements of the Newtonian calculation. However, the Divergence Theorem enables the analytic flux calculation to be mapped to an analytic divergence calculation. Since the traditional surface integration is only performed over the unshadowed surface of the vehicle, the analytic flux calculation must also only be performed over the unshadowed surface of the vehicle. As a result, the analytic divergence calculation must be performed throughout the unshadowed volume of the vehicle as shown in Figure 7 for an example hemisphere. Note that the shadow boundary occurs where $C_p = 0$, forming a plane for the hemisphere example.

As previously mentioned, only the flux across the unshadowed surface of the vehicle is used to calculate the force coefficients. However, the integration of the divergence of the mathematical vector field throughout the unshadowed volume is equivalent to the total flux across all enclosing boundaries. As such, the flux across any shadowed enclosing boundaries must be removed from the divergence solution. Since the magnitude of the mathematical vector field is equivalent to C_p as described in Eq. (7), the velocity of the mathematical vector field vanishes along the shadowed boundary where $C_p = 0$. As a result, the corresponding flux is identically zero along this boundary. Additionally, the shadowed boundary along the lower portion of the example hemisphere is parallel to the direction of the mathematical vector field as shown in Figure 8. As a result, the flux along this boundary is also identically zero. In summary, the flux corresponding to the normal force coefficient as described by Eq. (7) across the unshadowed surface of the example hemisphere is equivalent to the integral of the divergence of this flux throughout the unshadowed volume.

When computing additional aerodynamic coefficients, such as the axial force coefficient, the direction of the mathematical vector field changes as shown in Figure 9. To compute the axial force coefficient, the divergence of the new mathematical vector field is integrated throughout the unshadowed volume. While the flux is zero across the shadowed boundary where $C_p = 0$, the flux across the lower shadowed boundary is no longer zero. To accurately compute the axial force coefficient, the flux across this boundary must be removed from the divergence solution. While this method is mathematically correct, the analytic expression for the flux across the lower shadowed boundary is generally quite lengthy. This flux calculation resembles the surface integration performed by the traditional Newtonian method and as a result, reduces the compactness of the analytic expressions made possible by the Divergence Theorem.

This issue can be eliminated by extending the shadow plane to the maximum z-coordinate of the example hemisphere. An add-on volume can then be created by extending the lower portion of the hemisphere along the negative x-direction until the extended shadow plane is reached as shown in Figure 10. The surface created by this extension is parallel to the mathematical vector field, and as a result, the flux across this surface is zero. Since the flux along the shadowed plane where $C_p = 0$ is also zero, the integral of the divergence of the mathematical vector field throughout this add-on volume is equivalent to the flux across

American Institute of Aeronautics and Astronautics

the adjacent shadowed boundary shown in Figure 9. As such, the compactness of the analytic expressions made possible by the Divergence Theorem is fully realized using this approach. Note that the addition of these volumes would alter the aerodynamics when performing traditional Newtonian calculations since these volumes would alter the unshadowed surface of the vehicle. However, the direction of the mathematical vector field remains constant regardless of vehicle orientation and physical flow direction, allowing the construction of these additional volumes. While an example hemisphere is used, the general approach described in this section is applied to all divergence calculations where applicable.
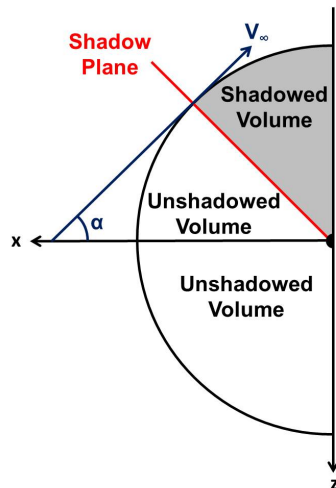

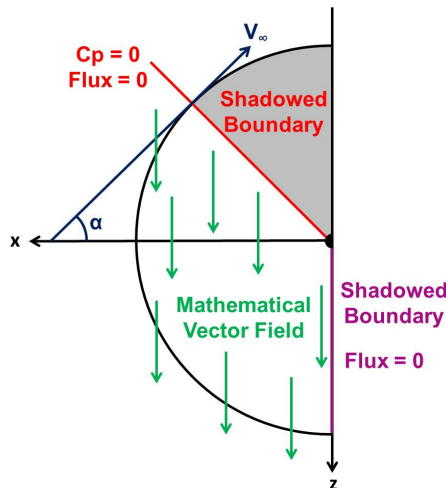**Figure 7. Shadowed and unshadowed volumes of hemisphere.**

Figure 8. Flux of mathematical vector field for normal force calculation of hemisphere.
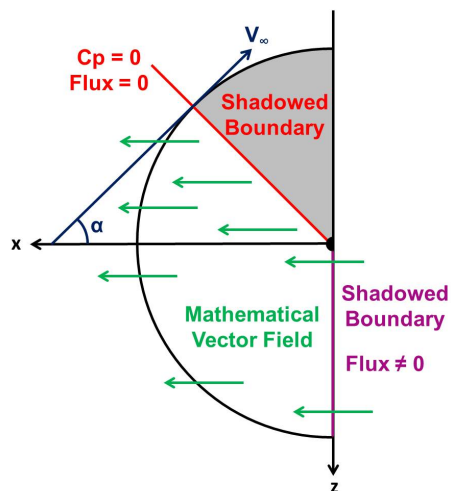

Figure 9. Flux of mathematical vector field for axial force calculation of hemisphere.
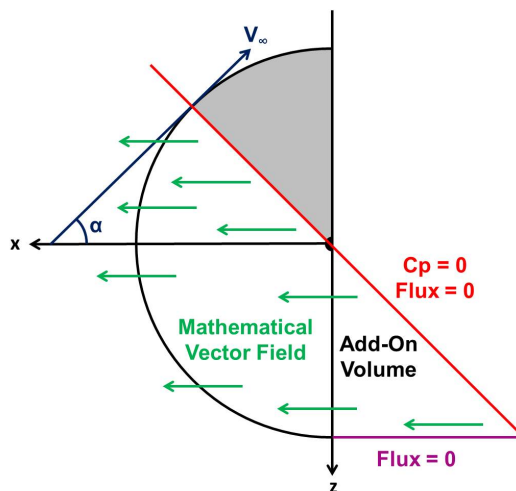

Figure 10. Flux of mathematical vector field with add-on volume for axial force calculation of hemisphere.

IV. Application of the Divergence Theorem to Select Examples

To illustrate the advancements in analytic aerodynamics made possible by the Divergence Theorem, several select examples are provided. First, a spherical segment is analyzed to describe the benefits in solution compactness that can be achieved with this approach. Second, more complex semi-spherical shapes are used to demonstrate that new analytic solutions can be obtained that are otherwise not possible when performing the traditional Newtonian calculation. Finally, parabolas of revolution provide an example of computationally efficient, hybrid exact-approximate solutions that are made possible using the Divergence Theorem. In the following examples, potential functions are used to describe each shape that is analyzed,

American Institute of Aeronautics and Astronautics

and Mathematica is used to perform the analytic integrations.

IV.A. Quadratic Potential Functions

The spherical potential shown in Eq. (11) has several simplifying properties that make it a useful starting point to implement the Divergence Theorem. As previously mentioned, the magnitude of the normal vector is constant across the entire surface of the shape. This potential recovery of the gradient shown in Eq. (12) eliminates the inverse trigonometric functions that result from normal vector normalizations as described in Section II. As a result, the divergence of the flux corresponding to the normal force coefficient can be expressed as shown in Eq. (13) for an assumed zero sideslip. This assumption eliminates y from the numerator for reasons that will be discussed in the following example, and this assumption is applied to all divergence calculations in this investigation. When analytically integrating the traditional Newtonian calculation, terms of the form $x^n\sqrt{1-x^2}$ appear, where n is even. These terms integrate to inverse trigonometric functions that add complexity to the integration process, resulting in the lengthy analytic aerodynamic expressions obtained in prior work.[28] Alternatively, the extra derivative of the integrand provided by the Divergence Theorem results in terms with a similar form where n is odd. These expressions eliminate the introduction of inverse trigonometric functions during the integration process, resulting in compact aerodynamic expressions. While the specific expressions for both the traditional and divergence calculations can be obtained from the aerodynamic database in Section I.B, the divergence calculation reduces the number of characters in the normal force coefficient by a factor of 24 and in the axial force coefficient by a factor of 15 when the add-on volume described in Section III is used. If the flux across the shadowed boundary is used instead of the add-on volume, then the length of the axial force coefficient expression is only reduced by a factor of 10.

$$\phi = x^2 + y^2 + z^2 = \rho^2 \tag{11}$$

$$|\nabla\phi| = \sqrt{4(x^2 + y^2 + z^2)} = 2\rho = 2\sqrt{\phi} \tag{12}$$

$$\nabla^T\mathbf{F} = \frac{-8\sin\alpha(-2x\cos\alpha - 2z\sin\alpha)}{4\phi} \tag{13}$$

Prior to integration, the unshadowed volume is divided into various regions. If these regions are not chosen carefully, then the limits of integration that define these regions may result in expressions that cannot be analytically integrated. After evaluating various options, a set of regions has been identified that enables the analytic integrations to be performed. This set has proven to be successful across all shapes included in this investigation. As an example, the quadratic potential of a hemisphere is divided into four regions. The first region is located in the forward section that is fully exposed to the flow as shown in Figure 11, and the fourth region consists of the entire lower section that is also fully exposed to the flow. Regions 2 and 3 fill the remaining unshadowed volume and are defined as shown in Figure 12 for an example cross-section of this remaining volume. Region 2 is bounded from above by the shadow plane whereas region 3 is bounded from above by the spherical shape. Note that these regions vary in size for each x location.
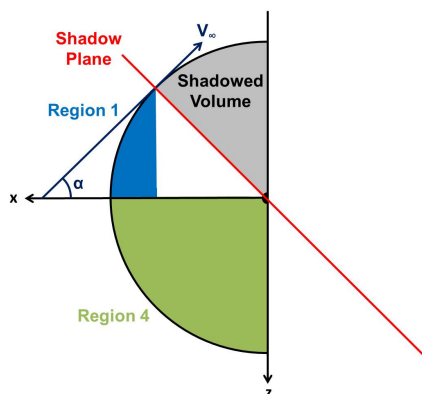

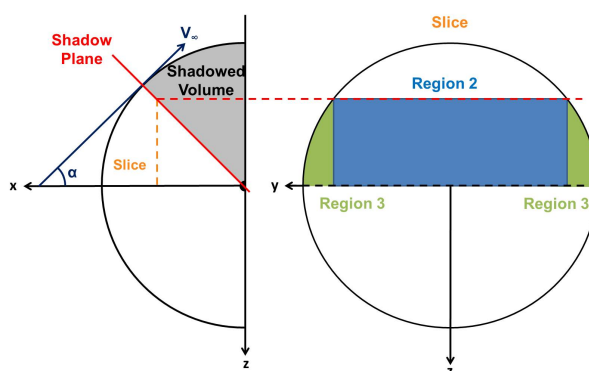Figure 11. Regions 1 and 4 for divergence integrations.

Figure 12. Regions 2 and 3 for divergence integrations.

American Institute of Aeronautics and Astronautics

These regions were also chosen to provide integration limits that naturally result from the choice in integration order. Many integration orders result in expressions that cannot be analytically integrated. The integration order of z, x, then y is chosen for this work. This order avoids the introduction of inverse trigonometric functions during the z and x integrations that generally prevent analytic solutions. Since y is the last integration to be performed, there is no concern if inverse trigonometric functions are introduced in this step. This integration order is also successfully used across many shapes in this investigation. The divergence solutions for the spherical segments described in Section II are validated using CBAERO as shown in Figure 13. Note that the analytic solution for the side force coefficient is identically zero as expected for a zero sideslip whereas numerical noise is present in the approximate solutions from CBAERO.
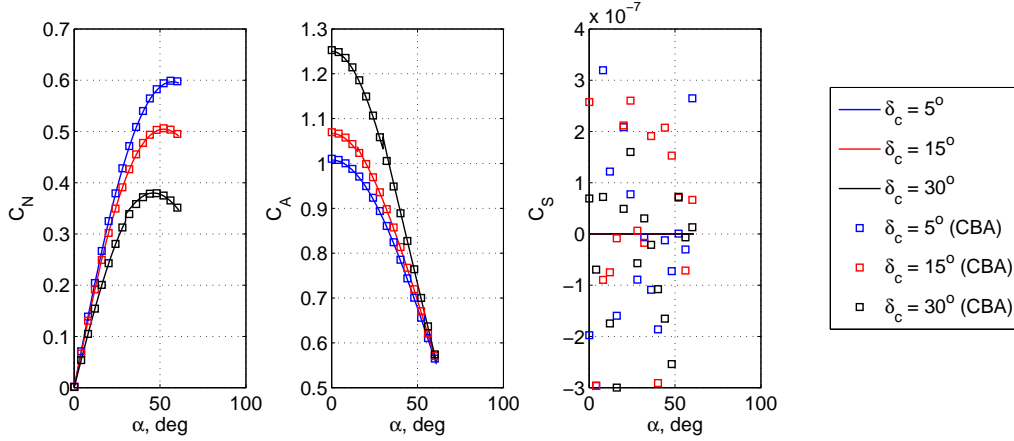

Figure 13. Comparison of spherical segment relations to CBAERO for various δ_c.

IV.B.   Semi-Quadratic Potential Functions

While the Divergence Theorem enables the construction of compact aerodynamic expressions, this technique also enables new solutions to be constructed that are otherwise not possible when performing the traditional Newtonian calculation as described in Section I. To obtain analytic solutions for more general shapes, the complexity of the spherical potential is increased as shown in Eq. (14), where c_{xz} is a constant. This form enables a partial recovery of the potential function in the gradient magnitude as shown in Eq. (15), where the magnitude is now a function of y and is denoted as $g(y)$. As a result, the expressions for the mathematical fluxes also increase in complexity as shown in Eq. (16) for the flux corresponding to the normal force calculation. The form of $g(y)$ was chosen to ensure that both x and z are absent from the gradient magnitude such that the added complexity of the gradient is delayed until the final integration is performed with respect to y.

$$\phi = c_{xz}x^2 + f(y) + c_{xz}z^2 = \rho^2 \tag{14}$$

$$|\nabla\phi| = \sqrt{4c_{xz}(\rho^2 - f(y)) + \left(\frac{\partial f(y)}{\partial y}\right)^2} = g(y) \tag{15}$$

$$\nabla^T \mathbf{F} = \frac{-8\sin\alpha(-2x\cos\alpha - 2z\sin\alpha)}{g(y)^2} \tag{16}$$

Initially, $f(y)$ is chosen as shown in Eq. (17) to maintain a quadratic potential, and the analytic relations for this family of shapes can be obtained from the aerodynamic database. The results for the shapes shown in Figure 14 are validated using CBAERO as shown in Figure 15. For non-axisymmetric bodies such as these, the GNU Triangulated Surface Library is used to construct the necessary meshes for evaluation in CBAERO.[10] Note that a singularity exists in these analytic relations for the spherical potential where $c_y = c_{xz}$. In this case, the prior analytic relations should be used instead.
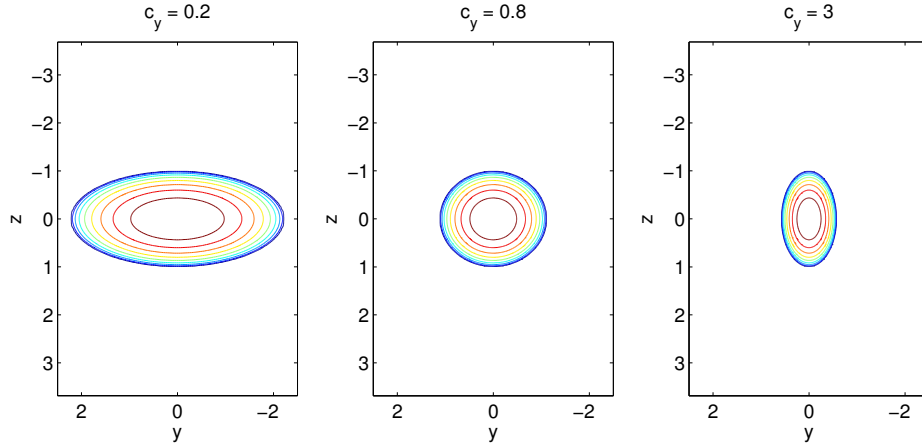
$$f(y) = c_y y^2 \tag{17}$$

Figure 14. Front view contours of shape for $f(y) = c_y y^2$ for various values of c_y.
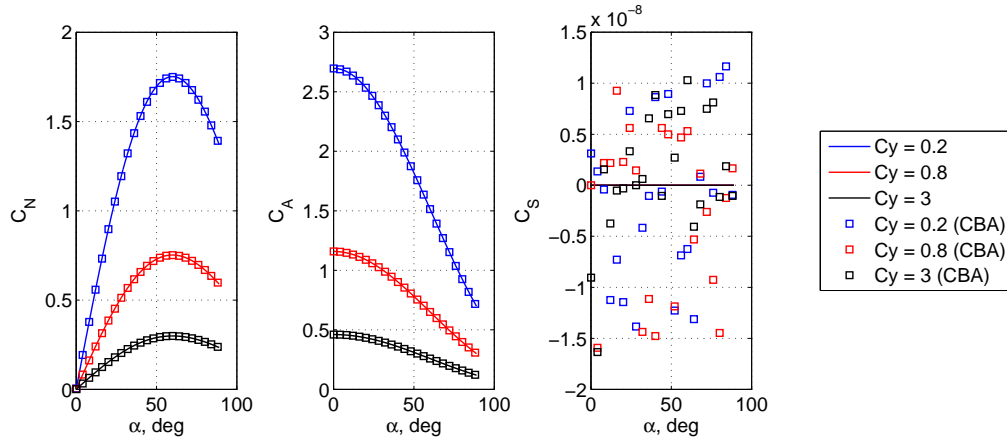

Figure 15. Comparison of quadratic relations to CBAERO for various values of c_y.

As many other candidate functions for $f(y)$ are evaluated, including expressions with various powers of y, trigonometric functions of y, etc., no analytic solution could be found. This mathematical limitation is a fundamental result of the normalization of vectors. As already shown in Eq. (15), $f(y)$ appears in two forms ($f(y)$ and $\frac{\partial f(y)}{\partial y}$) due to the normalization. When $f(y)$ is a quadratic function, both of these terms can be combined as a function of y^2. When any other power is used or when other functions are used, this simplification no longer applies, and the increased complexity of the normalization term prohibits an analytic solution. As a result, a mathematical limit in the analytic relations appears to have been reached for this class of shapes. However, the function $f(y) = e^{Ay+B} - e^B$ is an exception to this observation. The derivative property of this function results in a unique vector normalization in which terms of $f(y)$ can be combined using a complete-the-square technique. While the resulting analytic expressions in the database contain many individual imaginary terms, the combined result is purely real (to machine precision). Various configurations (shown in Figure 16 where $B = 0$) are validated using CBAERO as shown in Figure 17.

These results, in addition to the analytic solutions derived in prior work from traditional Newtonian calculations,[28] represent the current mathematical limit of exact solutions within the aerodynamic database. However, shapes outside of this exact database have solutions that can largely be represented with exact expressions and only require an approximation for a small portion of the solution. As such, the Divergence Theorem serves as the cornerstone to develop hybrid exact-approximate solutions. As each shape is divided into various regions as described in Section IV.A, an exact solution is found only if all integrations of each region can be performed analytically. For many shapes outside of the exact aerodynamic database, the majority of these regions can be integrated analytically and require no approximation. For the remain-
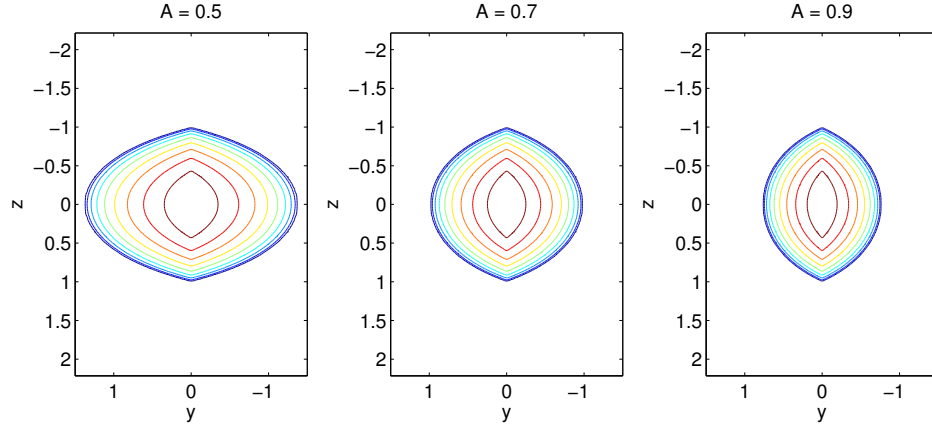
American Institute of Aeronautics and Astronautics

Figure 16. Front view contours of shape for $f(y) = e^{Ay+B} - e^B$ for various values of A.
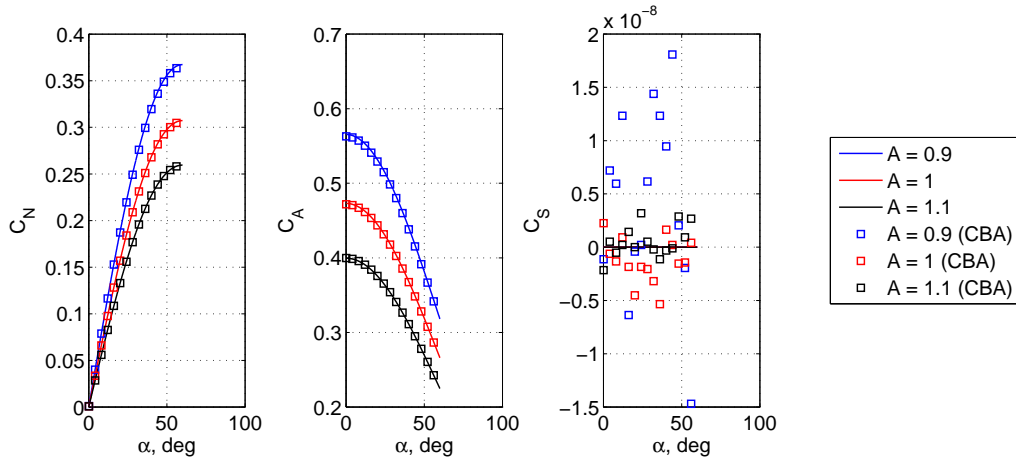

Figure 17. Comparison of quadratic exponential relations to CBAERO for various values of A.

ing regions, the first set of integrations can generally be performed analytically while the final integration must be approximated. If the expressions that must be approximated remain small relative to the exact expressions, then these hybrid exact-approximate solutions would likely serve as a computationally efficient approximation. As an example, the aerodynamic solution to a parabola of revolution is nearly exact and requires only a small set of expressions to be approximated.

IV.C. Parabola of Revolution

The parabola of revolution is described by the potential function shown in Eq. (18) with a gradient magnitude shown in Eq. (19). As illustrated, the potential recovery of the gradient is a function of x alone. As such, the integration order for this family of shapes is altered to z, y, then x to delay the introduction of inverse trigonometric functions until after the final integration. For this class of shapes, only the final integration in x of one term must be approximated for both the axial and normal force coefficients as shown in Eqs. (20) and (21), respectively, where the exact solutions can also be found in the aerodynamic database. Both of the terms that must be approximated originate from region 3 in which all other terms from this region can be exactly integrated. The limits of integration in x for this region are determined by the boundaries of region 3, where l is the length of the vehicle. Note that for this shape, the shadow boundary forms a plane that is parallel to the x-y plane. As a result, the add-on volume technique described in Section III cannot be used to simplify the flux through the base of the vehicle.

$$\phi = x + y^2 + z^2 = 0 \tag{18}$$

$$|\nabla\phi| = \sqrt{1 - 4x} \tag{19}$$

$$C_A = C_{A,exact} + \frac{2}{A_{ref}} \int_{-l}^{-1/4*\cot\alpha^2} -\frac{2x \arcsec\left(\frac{2}{\sqrt{4+\frac{\cot\alpha^2}{x}}}\right)(1 - x + (1 + x)\cos 2\alpha)}{(1 - 4x)^2} \, dx \tag{20}$$

$$C_N = C_{N,exact} + \frac{2}{A_{ref}} \int_{-l}^{-1/4*\cot\alpha^2} \frac{2x \arcsec\left(\frac{2}{\sqrt{4+\frac{\cot\alpha^2}{x}}}\right)\sin 2\alpha}{-1 + 4x} \, dx \tag{21}$$

Each expression that cannot be exactly integrated is approximated as a finite, analytic sum. As a result, the combined exact-approximate solutions are also fully analytic. This property allows vehicle shapes described by exact-approximate solutions to also be used within the rapid, simultaneous hypersonic aerodynamic and trajectory optimization framework described in Section I.A. Unlike panel methods, these expressions directly approximate the final aerodynamic result, and the error of this result can be directly controlled to obtain a desired accuracy. Alternatively, panel methods approximate vehicle shape to a certain level of accuracy, and the designer usually does not know *a priori* how this approximation translates to the accuracy of the aerodynamic coefficients. Consequently, multiple meshes of varying resolutions must be evaluated until convergence of the aerodynamic coefficients is observed. Using a trapezoidal approximation, the hybrid exact-approximate results for various parabolas of revolution with geometries shown in Figure 18 are validated using CBAERO as shown in Figure 19.
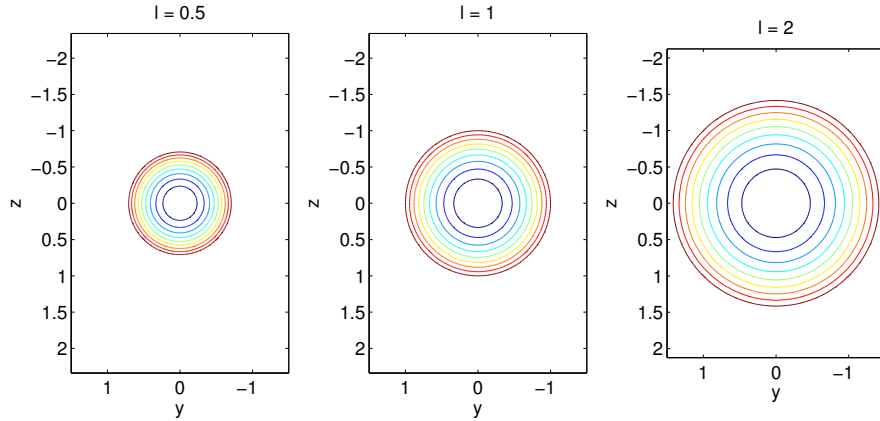

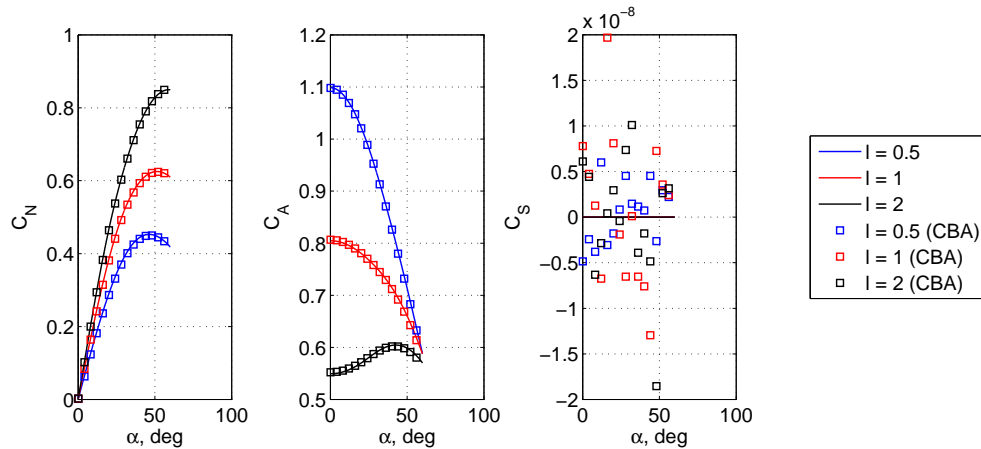Figure 18. Front view contours of shape for parabola of revolution for various values of l.

Figure 19. Comparison of parabola of revolution to CBAERO for various values of l.

American Institute of Aeronautics and Astronautics

There are likely many shapes with hybrid exact-approximate solutions. As more complex potential functions are investigated, the potential recovery technique of the gradient will likely no longer result in an expression that is a function of one variable, such as y as shown in Eq. (15). For example, the general spherical potential shown in Eq. (22) has a gradient magnitude shown in Eq. (23), where the potential recovery technique is only capable of eliminating a single variable (chosen to be x). To offset this added complexity, simplifying techniques can be used within certain regions of integration. For example, region 2 shown in Figure 12 is bounded above by the shadow plane where $C_p = 0$ and bounded below where $z = 0$. Since the divergence of the flux for the normal force coefficient is $\frac{dC_p}{dz}$, a first integration with respect to z would recover the pressure coefficient. As such, this expression vanishes along the upper boundary of region 2 where $C_p = 0$. Additionally, all instances of z vanish along the lower boundary where $z = 0$. These calculations eliminate z from the potential recovery expression in Eq. (23). As a result, this new expression takes the form of a single variable, y, allowing the remaining integrations to be carried forward in the same manner as before. Techniques such as these may be beneficial as the aerodynamic database is expanded to include hybrid exact-approximate solutions of more complex shapes.

$$\phi = c_x x^2 + c_y y^2 + c_z z^2 = \rho^2 \tag{22}$$

$$|\phi| = \sqrt{4(c_x^2 x^2 + c_y^2 y^2 + c_z^2 z^2)} = \sqrt{4c_x(\rho^2 - c_y y^2 - c_z z^2) + 4c_y^2 y^2 + 4c_z^2 z^2} \tag{23}$$

V.   Computational Advantages of the Analytic Aerodynamics

While all of the aforementioned analytic solutions enable the construction of a unified mathematical framework to perform rapid simultaneous hypersonic aerodynamic and trajectory optimization as described in Section I.A, these solutions could also serve as a computationally efficient substitute for panel methods within traditional design environments. A computational comparison between the analytic relations and CBAERO is shown in Figure 20. This comparison considers analytic solutions obtained from traditional Newtonian calculations in prior work[28] as well as the divergence solutions obtained in this investigation. A detailed description of the additional geometries considered within this comparison is provided in the prior work.[28]
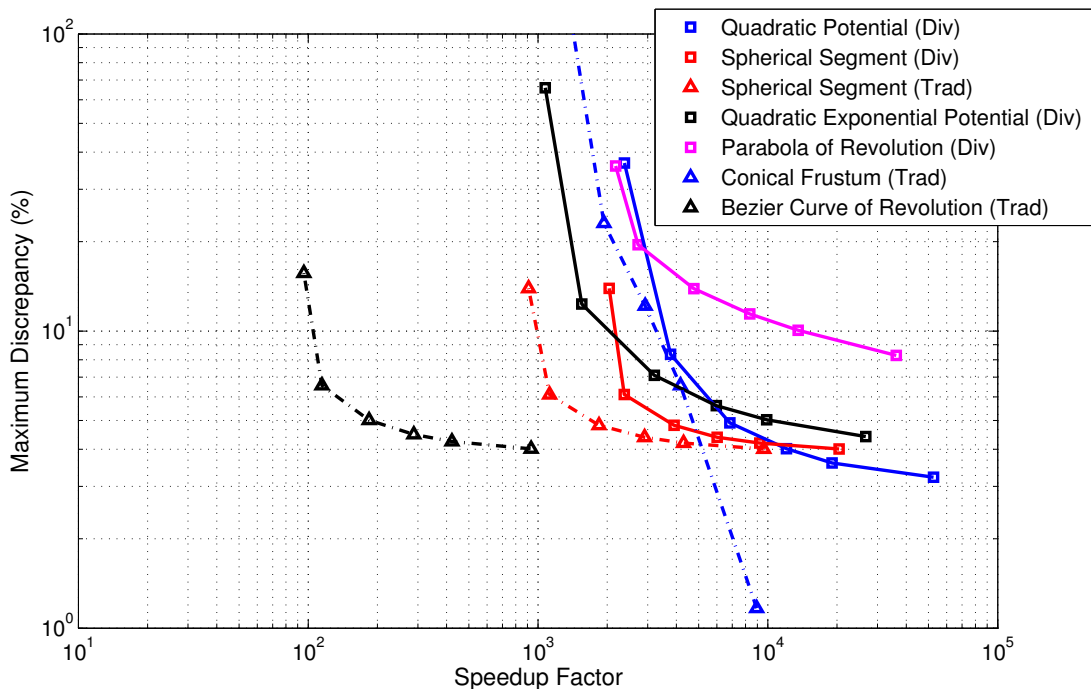

Figure 20. Maximum percent error in L/D vs. speedup of analytic aerodynamics.

American Institute of Aeronautics and Astronautics

For these data, the maximum discrepancy in a relevant design parameter, L/D, across varying angles of attack is shown for various CBAERO mesh resolutions. In this comparison, only L/D values greater than 0.01 are compared to avoid the L/D error singularity as α approaches zero. Note that the discrepancy shown in Figure 20 does not directly correspond to the numerical approximation error of CBAERO. CBAERO is performing many other calculations and is not directly approximating the analytic solutions. However, as the mesh resolution is made more fine, the CBAERO solutions increase in accuracy, and as a result, the discrepancy between the CBAERO solutions and the analytic solutions decrease. This accuracy benefit is attained at the increased computational cost of more panel calculations. Alternatively, the analytic relations provide an exact or nearly exact (*e.g.*, hybrid relations) solution to Newtonian flow theory, and the computational cost of evaluating each relation remains fixed.

For this comparison, a speedup factor is also calculated and is defined as the ratio of clock time between the evaluation of the analytic relations and the CBAERO calculations over a range of angles of attack for a single geometry. Since CBAERO is written in a compiled language, the Matlab-based analytic relations within the database are autocoded into C to make a reasonable comparison of clock times. Note that the speedup factor also includes the clock time necessary to generate the mesh of panels for CBAERO since this process would be required for any change in vehicle shape. Alternatively, the speedup factor does not include the time required to develop the analytic relations since this has already been performed for the shapes evaluated in Figure 20 and does not need to be repeated.

As shown in Figure 20, convergence in numerical accuracy of the CBAERO solutions is only observed for those shapes that show a maximum discrepancy that is largely insensitive to speedup factor (spherical segments and Bezier curves of revolution). While the other shapes do not display full convergence in numerical accuracy, the large speedups provided by the analytic relations would eliminate the usefulness of CBAERO calculations with higher mesh resolutions. As such, these higher resolutions were not included in the computational comparison. Note that even for large, unconverged discrepancies, many of the analytic relations still provide a speedup of approximately three orders of magnitude. This includes the example hybrid exact-approximate analytic solution (parabola of revolution), illustrating that further opportunities exist in this area. Bezier curves of revolution are the only exception to this observation due to the very lengthy analytic solutions obtained in the prior work. However, the analytic relations for these shapes still provide a speedup of two orders of magnitude. Additionally, greater speedup factors are observed for the divergence solution to the spherical segment as expected from the compact relations provided by this approach.

Note that for small speedup factors, large changes in discrepancy are observed for small changes in speedup factor. This is due to CBAERO calculations that are dominated by meshing algorithms that must be executed to construct the surface panels. For low mesh resolutions, this upfront cost is relatively constant and serves as a minimum time in which CBAERO can be executed. The conical frustum (described in the prior work) is in general more slender than the other shapes considered, and as a result, the numerical accuracy in L/D of these slender shapes greatly improves with higher mesh resolutions. Finally, when multiple geometries of the analytic relations are combined to construct hypersonic vehicles of interest as described in Section I.B, the speedup factor will be reduced accordingly. However, the combination of many traditional and divergence solutions will still provide a speedup of multiple orders of magnitude.

VI.   Future Work

The divergence solutions obtained in this investigation complement the relations obtained from the traditional Newtonian calculation in prior work.[28] As such, the divergence solutions could also serve the many potential applications in shape design, simultaneous vehicle and trajectory optimization, onboard guidance design, and aerodynamic modeling of shape change due to ablation as described in this prior work. The divergence solutions, along with the traditional Newtonian solutions, serve as the current theoretical limit of the analytic relations. However, the examples provided in this investigation serve as means to illustrate the benefits of the Divergence Theorem. Other mathematical techniques should also be considered to construct a library of Newtonian aerodynamic methods. As an example, moment calculations could potentially be converted into a circulation problem. This approach would allow Stoke's Theorem to be applied, and new or improved analytic moment solutions may be obtained using this technique.

Additional considerations should also be made with regard to vehicle parameterization, integration limits, and integration orders to capture new analytic solutions where possible. The various mathematical techniques should be assembled in an automated manner to support the widespread search for analytic solutions, and

a computational framework is being developed within a high performance computing cluster at Purdue University to perform this search. Special emphasis should be given to the construction of computationally efficient, compact solutions to support design and optimization studies. As solutions to new configurations are explored, special consideration should be given to emerging technologies such as morphing or flexible structures. For example, analytic relations for inflatable aerodynamic decelerators would enable the real-time modeling of shape change during trajectory propagation. As such, these relations could be used to improve the hypersonic modeling of passively flexible systems or to support targeting studies of actively controlled systems. Finally, analytic relations derived from fundamental models could also be obtained for non-Newtonian flow regimes such as free molecular flow to enable the rapid study of satellite orbital decay or trajectories of tumbling rocket bodies.[23]

VII.   Summary

In this investigation, analytic hypersonic force coefficients are developed through the application of the Divergence Theorem to Newtonian flow theory. To reduce the complexity of certain existing relations and to obtain analytic solutions for new configurations, the traditional Newtonian model is converted into a mathematically equivalent model of a flux that passes through an assumed permeable outer mold line of the vehicle. This technique enables the traditional surface integration to be converted into a volume integration of the divergence of the mathematical flux. While this conversion requires an additional integration to be performed, the integrand is sufficiently altered in a manner that simplifies the analytic calculation. For the examples shown, this simplification avoids the introduction of inverse trigonometric functions that often prevents the construction of analytic solutions. An example spherical segment illustrates the compact relations made possible by the Divergence Theorem in which the axial and normal force coefficients are compressed by a factor of 15 and 24, respectively. New analytic solutions of semi-quadratic potential functions are also made possible by the Divergence Theorem. These solutions, in addition to the traditional analytic solutions in prior work, represent the current limit in exact, analytic relations. For more complex configurations, a portion of the aerodynamics can be calculated exactly while the remaining terms require an approximation. The example parabola of revolution illustrates an efficient hybrid exact-approximate solution in which only one integrated term in each force coefficient must be approximated.

When applying the Divergence Theorem, each geometry is divided into multiple regions that are carefully chosen to provide a coordinated set of integration limits and integration order that leads to analytically integrable solutions. After this is accomplished for each geometry, the Divergence Theorem enables a wider range of simplifying mathematical techniques to be applied. In this investigation, compact analytic solutions are constructed by adjoining mathematically advantageous volumetric regions to the original geometry of interest. This technique is made possible by the constant direction of the mathematical vector field and is not available when performing the traditional Newtonian calculation. Additionally, simplifications to the analytic integrations are made for regions that are adjacent to the shadow boundary where the mathematical flux vanishes.

By combining the various geometries that currently exist within the analytic aerodynamic database, hypersonic vehicles of interest can be rapidly evaluated to support conceptual design and optimization studies. As such, these relations could substitute approximate panel methods widely used in traditional, segregated conceptual design environments. Comparisons with a state-of-the-art paneling tool, CBAERO, illustrate the three to four orders of magnitude reduction in computational resources enabled by many of the analytic relations. More importantly, however, these relations eliminate the large aerodynamic tables that fundamentally segregate aerodynamics from other analyses during conceptual design. The additional and improved analytic relations obtained by the Divergence Theorem enable a wider range of hypersonic vehicles to be included within the unified, mathematical design framework made possible by the development of analytic aerodynamic relations.

References

[1]Newton, I., *Principia - Motte's Translation Revised*, University of California Press, 1946.

[2]Anderson, J. D., *Hypersonic and High Temperature Gas Dynamics*, AIAA, 1989.

[3]Kinney, D. J., "Aero-Thermodynamics for Conceptual Design," AIAA-2004-31-962, *42nd AIAA Aerospace Sciences Meeting and Exhibit*, Reno, NV, 5-8 Jan. 2004.

[4]Bonner, E., Clever, W., and Dunn, K., "Aerodynamic Preliminary Analysis System II: Part I Theory," *NASA-CR-165627*,

Apr. 1981.

[5]Smyth, D. N. and Loo, H. C., "Analysis of Static Pressure Data from 1/12-scale Model of the YF-12A. Volume 3: The MARK IVS Supersonic-Hypersonic Arbitrary Body Program, User's Manual," *NASA-CR-151940*, Oct. 1981.

[6]Cunningham, M., "Hypersonic Aerodynamics for an Entry Research Vehicle," *Journal of Spacecraft and Rockets*, Vol. 24, No. 2, 1987.

[7]Rainey, R. W., "Working Charts for Rapid Prediction of Force and Pressure Coefficients on Arbitrary Bodies of Revolution by Use of Newtonian Concepts," *NASA TN D-176*, 1959.

[8]Margolis, K., "Theoretical Evaluation of the Pressures, Forces, and Moments at Hypersonic Speeds Acting on Arbitrary Bodies of Revolution Undergoing Separate and Combined Angle-of-Attack and Pitching Motions," *NASA TN D-652*, 1961.

[9]Grimminger, G., Williams, E. P., and Young, G. B. W., "Lift on Inclined Bodies of Revolution in Hypersonic Flow," *Journal of the Aeronautical Sciences*, Vol. 17, No. 11, 1950.

[10]GTS Library Reference Manual, http://gts.sourceforge.net/reference/book1.html.

[11]Hoffman, S. J. and Kaplan, D. I., "Human Exploration of Mars: The Reference Mission of the NASA Mars Exploration Study Team," *NASA Special Publication 6107*, July 1997.

[12]Drake, B. G., "Reference Mission Version 3.0 Addendum to the Human Exploration of Mars: The Reference Mission of the NASA Mars Exploration Study Team," *NASA Special Publication 6107-ADD*, June 1998.

[13]Steinfeldt, B., Theisinger, J., Korzun, A., Clark, I., Grant, M., and Braun, R., "High Mass Mars Entry Descent and Landing Architecture Assessment," AIAA 2009-6684, *AIAA Space 2009*, Pasadena, CA, 14 - 17 Sept. 2009.

[14]Desai, P., Lyons, D., Tooley, J., and Kangas, J., "Entry, Descent, and Landing Operations Analysis for the Stardust Entry Capsule," *Journal of Spacecraft and Rockets*, Vol. 45, No. 6, 2008.

[15]Desai, P. and Lyons, D., "Entry, Descent, and Landing Operations Analysis for the Genesis Entry Capsule," *Journal of Spacecraft and Rockets*, Vol. 45, No. 1, 2008.

[16]Kinney, D. J. and Bowles, J. V., "Conceptual Design of a 'SHARP'-CTV," AIAA 2001-2887, *35th AIAA Thermophysics Conference*, Anaheim, CA, 11-14 Jun. 2001.

[17]Grant, M. J., Clark, I. G., and Braun, R. D., "Rapid Design Space Exploration for Conceptual Design of Hypersonic Missions," *AIAA Atmospheric Flight Mechanics Conference and Exhibit*, Portland, OR, 8-11 Aug. 2011.

[18]Grant, M. J., Clark, I. G., and Braun, R. D., "Rapid Simultaneous Hypersonic Aerodynamic and Trajectory Optimization Using Variational Methods," *AIAA Atmospheric Flight Mechanics Conference and Exhibit*, Portland, OR, 8-11 Aug. 2011.

[19]Wells, W. and Armstrong, W., "Tables of Aerodynamic Coefficients Obtained From Developed Newtonian Expressions for Complete and Partial Conic and Spheric Bodies at Combined Angles of Attack and Sideslip with Some Comparisons with Hypersonic Experimental Data," *NASA TR R-127*, 1962.

[20]Eggers, A. J., Resnikoff, M. M., and Dennis, D. H., "Bodies of Revolution Having Minimum Drag at High Supersonic Airspeeds," *NACA TR-1306*, 1957.

[21]Elsgloc, L. D., *Calculus of Variations*, Dover Publications, Inc., 2007.

[22]Auman, L. M. and Wilks, B., "Supersonic and Hypersonic Minimum Drag for Bodies of Revolution," *AIAA 21st Applied Aerodynamics Conference*, Orlando, FL, 23-26 Jun. 2003.

[23]Regan, F. J. and Anandakrishnan, S. M., *Dynamics of Atmospheric Re-Entry*, AIAA, 1993.

[24]Theisinger, J. E. and Braun, R. D., "Multi-Objective Hypersonic Entry Aeroshell Shape Optimization," *Journal of Spacecraft and Rockets*, Vol. 46, No. 5, 2009.

[25]Kinney, D. J., "Aerodynamic Shape Optimization of Hypersonic Vehicles," AIAA 2006-239, *44th AIAA Aerospace Sciences Meeting and Exhibit*, Reno, NV, 9-12 Jan. 2006.

[26]Mathematica, Ver. 7, Wolfram Research, Champaign, IL.

[27]Maple, Ver. 13, Waterloo Maple Inc., Waterloo, Ontario, Canada.

[28]Grant, M. J. and Braun, R. D., "Analytic Hypersonic Aerodynamics for Conceptual Design of Entry Vehicles," *48th AIAA Aerospace Sciences Meeting Including the New Horizons Forum and Aerospace Exposition*, Orlando, FL, AIAA 2010-1212, 4-7 Jan. 2010.

[29]Anderson, Jr., J. D., *Fundamentals of Aerodynamics*, McGraw-Hill, 2001.

[30]George B. Thomas, J. and Finney, R. L., *Calculus*, Addison-Wesley Publishing Company, 1996.